Scattering-matrix analysis of periodically patterned multilayers with asymmetric unit cells and birefringent media

Marco Liscidini,[1] Dario Gerace,[2] Lucio Claudio Andreani,[3] and J. E. Sipe[1]
[1]*Department of Physics, University of Toronto, 60 St. George Street, Ontario, Canada M5S 1A7*
[2]*Institute of Quantum Electronics, ETH Zurich, 8093 Zurich, Switzerland*
[3]*Department of Physics "A. Volta", University of Pavia, Via Bassi 6, I-27100 Pavia, Italy*
(Received 4 September 2007; revised manuscript received 31 October 2007; published 18 January 2008)

Fourier analysis has been successfully applied to study optical properties of photonic crystal structures, usually composed of optically isotropic media. In a commonly used formulation [D. M. Whittaker and I. S. Culshaw, Phys. Rev. B **60**, 2610 (1999)], inversion symmetry of the unit cell is required. Here, we extend the treatment of Whittaker and Culshaw to structures with asymmetric unit cells that can be composed of birefringent media. As applications we consider a high-refractive-index membrane with a triangular lattice of triangular holes, where the presence of a TE-like gap at ω and of a TM-like gap at 2ω is established, and a slot waveguide made of (birefringent) porous silicon, where coupling of guided modes to radiative modes is achieved through a one-dimensional periodic grating.

DOI: 10.1103/PhysRevB.77.035324 PACS number(s): 78.20.Bh, 78.67.−n, 42.70.Qs

I. INTRODUCTION

Periodically patterned multilayer photonic structures, such as photonic crystal slabs or membranes, are very promising systems for the realization of integrated optical devices, especially low loss waveguides and high Q cavities.[1,2] The theoretical analysis of such structures is complicated when the effects of external coupling or emission by internal sources have to be considered. The in-plane periodicity suggests a field description by means of a Fourier method, where the problem is treated in reciprocal space instead of direct space. Such treatments, initially developed for the theory of gratings in diffractive optics,[3,4] have been extended and applied to the study of photonic crystal structures.[5–9] Once the expression of the field is obtained in terms of its Fourier components, boundary conditions at the interface between different spatial regions are usually imposed by means of a scattering-matrix approach originally developed for the study of electron transmission in semiconductor heterostructures.[10] The calculations are accurate and fast, and nowadays can easily be performed on a standard personal computer. A scattering-matrix treatment along these lines has been developed in detail by Whittaker and Culshaw.[11] It can be used to solve Maxwell's equations for a realistic patterned multilayer, to evaluate reflectance and transmittance spectra, and to calculate the emission from an internal dipole source. Even though this method is a very powerful and efficient tool, its original formulation[11] requires inversion symmetry of the unit cell of the periodic pattern, and birefringent materials are not treated.

Recently, a photonic crystal slab with a triangular lattice of triangular air holes has been identified as a structure for which a photonic band gap for both polarizations can be achieved.[12] Indeed, in this system, it is possible to obtain several photonic gaps for odd modes (quasi-TM polarization) besides the usual gap for the fundamental even (quasi-TE polarization) mode.[13] These properties make the system appealing for applications in nonlinear optics, for example, in achieving doubly resonant second-harmonic generation, as studied in one- and two-dimensional systems.[14–18] Unfortunately, the lack of inversion symmetry of a triangular hole prevents a description of such a structure by means of the scattering-matrix method.[11]

In another recent development, porous silicon (PSi) has attracted growing interest due to the possibility of obtaining visible light emission at room temperature.[19] This material offers easy fabrication of high quality one-dimensional photonic crystal structures and planar waveguides, thanks to the strong dependence of the refractive index on porosity.[20,21] Because of the possibility of growing structures with a large number of layers, many interesting phenomena have already been explored in PSi multilayers, such as second-harmonic generation in coupled microcavities and light localization in disordered systems.[22,23] The possibility of infiltrating PSi structures with other materials suggests the use of those devices for biosensing, and several examples of PSi based sensors have already been proposed.[24–26]

In many porous silicon structures, the pore size is smaller than the wavelength of light, and the material can be treated by effective medium theory, in which an effective dielectric tensor is associated with a mesoscopic volume of the structure containing many pores. Although bulk silicon itself is optically isotropic, the effective medium is naturally birefringent due to preferential etching of the pores in the vertical direction.[27] A simple planar waveguide composed of isotropic media can also be characterized by a sort of birefringence due to the different degree of field confinement for the two polarizations: this happens, in particular, in the so-called slot waveguides.[28,29] This effect can be called "form birefringence," since it depends on the geometrical properties of the systems; it has been proposed as an efficient method for achieving phase matching in multilayer waveguides of cubic materials, where natural birefringence cannot be exploited.[30,31] In the case of a photonic crystal or a waveguide made of PSi, the optical response is determined by the combination of natural birefringence of the constituent media and form birefringence of the whole structure. Although a birefringent one-dimensional system can be efficiently de-

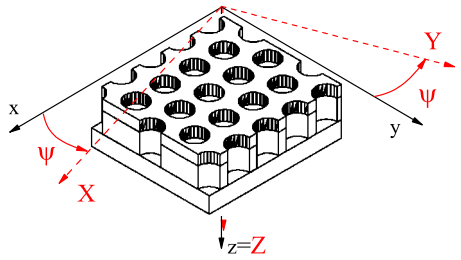

FIG. 1. (Color online) Scheme of a periodically patterned multilayer: laboratory reference system and principal dielectric axes are indicated with continuous and dashed lines, respectively. We treat the case in which the growth direction is along the axis Z. The laboratory reference system Σ_{xyz} is obtained from Σ_{XYZ} through a clockwise rotation of an angle ψ around Z.

scribed by means of a transfer matrix formalism,[32] when an in-plane periodic pattern is introduced (as in the case of a photonic crystal slab or grating coupled waveguide), this method could become numerically unstable. A description by means of a scattering matrix is possible, but the natural medium birefringence must be taken into account in the formalism.

In this work, we propose two extensions of the scattering-matrix method[11] to describe systems in which there is no center of inversion symmetry of the unit cell, or which are composed of birefringent materials. The paper is organized as follows: In Sec. II, we present the generalization of the method to treat asymmetric unit cells; we discuss in detail the symmetry properties of the matrices that are involved in the construction of the total scattering matrix. The issue of birefringent materials is studied in Sec. III, where a further generalization of the method is presented. Applications are presented in the following two sections: In Sec. IV, the formalism is utilized to characterize a high-refractive-index membrane with a triangular lattice of triangular holes, and in Sec. V, we present numerical results for a PSi slot waveguide. We point out that, when the cell has inversion symmetry and no birefringent materials are considered, the present formulation coincides with the one in Ref. 11. Thus, throughout the paper we maintain, wherever possible, the same notation and terminology as in Ref. 11 as summarized in the Appendix.

II. SCATTERING-MATRIX METHOD FOR UNIT CELLS WITHOUT INVERSION SYMMETRY

The procedure for building the scattering matrix of a planar periodically patterned system (see Fig. 1) can be summarized as follows: (i) The electromagnetic waves are expanded in a plane-wave set and Maxwell's equations are written in the in-plane momentum representation; (ii) the band structure of each patterned layer, taken to be homogeneous in the z direction, is evaluated, yielding a set of states $\{\phi_i\}$ describing propagation in the z direction as simple plane waves, $\exp(iq_iz)$; (iii) the electromagnetic field is expanded in terms of these forward and backward Bloch states; (iv) the scattering matrix is found by means of an iterative procedure in which the continuity of the tangential components of the electric and magnetic fields at the interfaces between the different layers is required.

The crucial point of the entire method is finding, for each layer, an appropriate set of basis functions $\{\phi_i\}$ and the corresponding wave vector components q_i along the z direction. A natural starting point is to expand the magnetic field in basis states with zero divergence, so that the condition $\nabla \cdot \mathbf{H}=0$ is automatically satisfied. Then the Fourier expansion coefficients for each function ϕ_i, and the corresponding q_i, follow from Maxwell's equations in the momentum representation. They are determined from the solution of the eigenvalue problem

$$\Gamma \phi_i = q_i^2 \phi_i, \tag{1}$$

where

$$\Gamma = [\mathcal{E}(\omega^2 - \mathcal{K}) - K].$$

Here, $\mathcal{E}$, $\mathcal{K}$, and K are $2N \times 2N$ matrices, where N indicates the number of reciprocal lattice vectors considered. The properties of these matrices depend on the Fourier transform of the dielectric function $\boldsymbol{\epsilon}(\mathbf{r})$, which is a periodic function in the plane and, for a given layer, it is assumed to be uniform along z. The expressions of all the operators can be found in Ref. 11 or, alternatively, in Eq. (A10) of the Appendix. The matrix $\hat{\varepsilon}$, which is contained in $\mathcal{E}$ and $\mathcal{K}$, is defined as

$$\hat{\varepsilon}_{ij} = \frac{1}{S} \int_{\text{cell}} \boldsymbol{\epsilon}(\mathbf{r}) e^{i(\mathbf{G}_i - \mathbf{G}_j)\cdot \mathbf{r}} d\mathbf{r}, \tag{2}$$

where $\mathbf{G}_i$ and $\mathbf{G}_j$ are reciprocal lattice vectors and S is the unit cell area. In this section, we assume, following Ref. 11, that the material is optically isotropic. We generalize this assumption in the next section.

While the solution of Eq. (1) does not require any particular assumption on the nature of the unit cell, the eigenvectors satisfy interesting properties that follow directly from the unit cell symmetry and the dielectric function nature. We will briefly discuss these properties and how they are related to some orthogonality relations that can be demonstrated for the eigenvectors $\{\phi_i\}$. It is straightforward to show that for a unit cell with inversion symmetry the matrix $\mathcal{E}$ is symmetric and the eigenvalue problem (1) can be reduced to the form of a generalized symmetric problem [see Eq. (A11)]. In this case, it is possible to find a set of eigenvectors for which the elements ϕ_i satisfy the particular orthogonality relations

$$\phi_i^T (\omega^2 - \mathcal{K}) \phi_j = \delta_{ij}. \tag{3}$$

When the unit cell lacks inversion symmetry and the dielectric function is real, the matrix $\hat{\varepsilon}$ (and therefore $\mathcal{E}$) is Hermitian and Eq. (1) can be rewritten in the form of a generalized Hermitian problem. For an asymmetric unit cell, the eigenvectors satisfy a more generalized orthogonality relation,

$$\phi_i^\dagger (\omega^2 - \mathcal{K}) \phi_j = \delta_{ij}, \tag{4}$$

where $\phi_i^\dagger$ indicates the adjoint of the vector. Finally, when the unit cell is not symmetric and the dielectric function is complex, nothing can be inferred about the eigenvector orthogonality. All the cases are summarized in Table I.

TABLE I. Properties of the Fourier transform of the dielectric function: the matrix $\hat{\varepsilon}$ is symmetric for a unit cell having inversion symmetry and, more generally, it is Hermitian when the dielectric function is real.

$\epsilon(\mathbf{r})$	Real	Complex
Symmetric	$\hat{\varepsilon}_{ij}=\hat{\varepsilon}_{ji}$	$\hat{\varepsilon}_{ij}=\hat{\varepsilon}_{ji}$
Asymmetric	$\hat{\varepsilon}_{ij}=\hat{\varepsilon}_{ji}^{*}$	—

We envision constructing the scattering matrix in the most general case, when neither the unit cell nor the dielectric function are assumed to have particular properties. We show below that the standard method has to be modified where it employs the orthogonality relation (3), which requires inversion symmetry for the unit cell, to construct the interface matrix that relates the field amplitudes of two adjacent layers.

Once the eigenvalue problem for a layer is solved, the Fourier components of the electromagnetic field can be expanded using the basis $\{\phi_i\}$. The relation between the expansion coefficients and the field components can be expressed by introducing the matrix M, defined as

$$\begin{pmatrix} e_{\parallel}(z) \\ h_{\parallel}(z) \end{pmatrix} = \begin{pmatrix} (\omega^2-\mathcal{K})\Phi\hat{q}^{-1} & -(\omega^2-\mathcal{K})\Phi\hat{q}^{-1} \\ \Phi & \Phi \end{pmatrix} \times \begin{pmatrix} \hat{f}(z)a \\ \hat{f}(d-z)b \end{pmatrix} \equiv M \begin{pmatrix} \hat{f}(z)a \\ \hat{f}(d-z)b \end{pmatrix}, \tag{5}$$

where $e_{\parallel}(z)$ and $h_{\parallel}(z)$ contain the (x,y) components of the fields, a and b are $2N$-dimensional vectors that contain the expansion coefficients, $\hat{q}$ is the diagonal matrix with $\hat{q}_{ii}=q_i$, Φ is the matrix whose columns are the vectors ϕ_i, and $\hat{f}(z)$ and $\hat{f}(d-z)$ are diagonal matrices, which take into account the field phase shift due to the propagation in the layer (see the Appendix).

In order to obtain an expression for the generic interface matrix between the layers l and $l+1$, we impose continuity of the tangential field components at the interface, and thus, the amplitudes (a_l,b_l) and (a_{l+1},b_{l+1}) satisfy the relation

$$\begin{pmatrix} \hat{f}_l a_l \\ b_l \end{pmatrix} = I(l,l+1) \begin{pmatrix} a_{l+1} \\ \hat{f}_{l+1} b_{l+1} \end{pmatrix}. \tag{6}$$

The interface matrix is related to the layer matrices M_l and M_{l+1} by the simple equation

$$I(l,l+1) = M_l^{-1} M_{l+1}. \tag{7}$$

The numerical inversion of the matrices M_l requires considerable effort, since each one of them is a $4N\times 4N$ matrix, and N typically varies from 31 to 109 or more in accurate simulations. In the original formulation of the scattering matrix method,[11] the interface matrix $I(l,l+1)$ is evaluated by constructing an explicit expression for M_l^{-1} [see Eq. (A14)], based on the orthogonality relation (3) that the set of eigenvectors $\{\phi_i\}$ satisfy. This strategy is not available if the unit cell lacks inversion symmetry, but it can easily be generalized when the dielectric function is real. Based on the orthogonality relation (4), we find that each M^{-1} can be written as

$$M^{-1} = \frac{1}{2} \begin{pmatrix} \hat{q}\Phi^{\dagger} & \Phi^{\dagger}(\omega^2-\mathcal{K}) \\ -\hat{q}\Phi^{\dagger} & \Phi^{\dagger}(\omega^2-\mathcal{K}) \end{pmatrix}, \tag{8}$$

where $\Phi^{\dagger}=(\Phi^{*})^{T}$ indicates the adjoint of Φ. Then the interface matrix is easily constructed:

$$I(l,l+1) = \frac{1}{2}\hat{q}_l\Phi_l^{\dagger}(\omega^2-\mathcal{K}_{l+1})\Phi_{l+1}\hat{q}_{l+1}^{-1} \begin{pmatrix} 1 & -1 \\ -1 & 1 \end{pmatrix} + \frac{1}{2}\Phi_l^{\dagger}(\omega^2-\mathcal{K}_l)\Phi_{l+1} \begin{pmatrix} 1 & 1 \\ 1 & 1 \end{pmatrix}. \tag{9}$$

For a unit cell lacking inversion symmetry and a complex dielectric function where no orthogonality relations are available, a more general approach is required. Still, rather than numerically inverting M, we can notice that it is possible to write

$$M = \begin{pmatrix} A & -A \\ B & B \end{pmatrix}, \tag{10}$$

where $A=(\omega^2-\mathcal{K})\Phi\hat{q}^{-1}$ and $B=\Phi$. Then M^{-1} can be constructed according to

$$M^{-1} = \frac{1}{2} \begin{pmatrix} A^{-1} & B^{-1} \\ -A^{-1} & B^{-1} \end{pmatrix}, \tag{11}$$

where $A^{-1}=q\Phi^{-1}(\omega^2-\mathcal{K})^{-1}$ and $B^{-1}=\Phi^{-1}$. The direct problem of inverting a $4N\times 4N$ matrix is then replaced by inverting two $2N\times 2N$ matrices, which still gives considerable saving in time.

These generalizations of the original scattering-matrix method[11] are useful in that the method is now suitable for any periodic pattern and, if the dielectric function is real, a structure with a unit cell without inversion symmetry is only marginally more complicated than the one with inversion symmetry. We illustrate this in Sec. IV below, but first we consider the further generalization to a structure consisting of birefringent media.

III. SCATTERING-MATRIX METHOD FOR BIREFRINGENT MEDIA

While in an isotropic medium the induced polarization is parallel to the electric field, this is not true for anisotropic media, except for particular propagation directions and polarizations. If we want to use the scattering-matrix method to describe a patterned multilayer containing one or more birefringent layers (even if the unpatterned ones), we must generalize the eigenvalue problem (1) to take into account the material anisotropy.

For each medium the relation between the electric field and the displacement vector can be written as

$$\begin{pmatrix} D_x \\ D_y \\ D_z \end{pmatrix} = \begin{pmatrix} \epsilon_{xx} & \epsilon_{xy} & \epsilon_{xz} \\ \epsilon_{yx} & \epsilon_{yy} & \epsilon_{yz} \\ \epsilon_{zx} & \epsilon_{zy} & \epsilon_{zz} \end{pmatrix} \begin{pmatrix} E_x \\ E_y \\ E_z \end{pmatrix}, \tag{12}$$

where ϵ_{ij} are complex numbers, and x, y, and z are the coordinates in the laboratory reference system Σ_{xyz}. We are assuming that Eq. (12) holds at any point in space, i.e., spatial dispersion effects are neglected. While a general extension of the scattering-matrix method for all possible symmetries of the dielectric tensor is complicated, we specify the treatment to two different situations that are described below.

In the first case, we assume that the dielectric tensor is diagonal with respect to fixed principal axes. This situation corresponds to most crystal symmetries, with the exception of monoclinic and triclinic crystallographic point groups. Moreover, we assume that one of the principal axes coincides with the growth axis z of the multilayer. The dielectric tensor can then be written as

$$\boldsymbol{\epsilon}(\mathbf{r}) = \begin{pmatrix} \epsilon_X(\mathbf{r}) & 0 & 0 \\ 0 & \epsilon_Y(\mathbf{r}) & 0 \\ 0 & 0 & \epsilon_Z(\mathbf{r}) \end{pmatrix} \tag{13}$$

and each of the diagonal components can be either real or complex. In particular, for uniaxial materials where the z axis coincides with the optic axis, $\epsilon_X = \epsilon_Y$. This situation corresponds to the case of nanoporous silicon layers, where the birefringence is determined by the fabrication process. The nanopores can be treated as cylindrical holes oriented in the z direction, and the dielectric constants parallel and perpendicular to the surface can be evaluated by means of Maxwell-Garnett-type effective medium theory.[27]

The eigenvalue equation that arises can be found by extending the procedure of Whittaker and Culshaw:[11] Using their notations and field rescaling (see the Appendix), we rewrite the equation $\nabla \times \mathbf{H} = -i\boldsymbol{\epsilon}\mathbf{E}$ in the momentum representation:

$$\begin{aligned} i\hat{k}_y h_z(z) - h_y'(z) &= -i\hat{\varepsilon}_X e_x(z), \\ h_x'(z) - i\hat{k}_x h_z(z) &= -i\hat{\varepsilon}_Y e_y(z), \\ i\hat{k}_x h_y(z) - i\hat{k}_y h_x(z) &= -i\hat{\varepsilon}_Z e_z(z), \end{aligned} \tag{14}$$

where we have introduced the matrices $\hat{\varepsilon}_\alpha$, with $\alpha = X$, Y, and Z, which are found using Eq. (2) for each component of the dielectric tensor. Choosing the usual expansion for the magnetic field

$$\mathbf{h}(z) = e^{iqz}\left\{ \phi_x \hat{\mathbf{x}} + \phi_y \hat{\mathbf{y}} - \frac{1}{q}(\hat{k}_x \phi_x + \hat{k}_y \phi_y)\hat{\mathbf{z}} \right\}, \tag{15}$$

we obtain the expression for the electric field Fourier components

$$\begin{aligned} \mathbf{e}(z) = \frac{1}{q} e^{iqz} \{ & \hat{\eta}_X [\hat{k}_y \hat{k}_x \phi_x + (q^2 + \hat{k}_y \hat{k}_y)\phi_y]\hat{\mathbf{x}} \\ & - \hat{\eta}_Y [\hat{k}_x \hat{k}_y \phi_y + (q^2 + \hat{k}_x \hat{k}_x)\phi_x]\hat{\mathbf{y}} \\ & + q\,\hat{\eta}_Z [\hat{k}_y \phi_x - \hat{k}_x \phi_y]\hat{\mathbf{z}} \}, \end{aligned} \tag{16}$$

where we have indicated with $\hat{\eta}_\alpha$ the inverse of the matrix $\hat{\varepsilon}_\alpha$. Equation (16) takes the place of Eq. (A8) in the original formulation.[11] Finally, using the new expressions for the electric field in the equation $\nabla \times \mathbf{E} = i\omega^2 \mathbf{H}$, we obtain a new eigenvalue problem for ω:

$$\begin{aligned} \left\{ \begin{pmatrix} \hat{\eta}_X & 0 \\ 0 & \hat{\eta}_Y \end{pmatrix} \left[q^2 + \begin{pmatrix} \hat{k}_x \hat{k}_x & \hat{k}_x \hat{k}_y \\ \hat{k}_y \hat{k}_x & \hat{k}_y \hat{k}_y \end{pmatrix} \right] \right. \\ \left. + \begin{pmatrix} \hat{k}_y \hat{\eta}_Z \hat{k}_y & -\hat{k}_y \hat{\eta}_Z \hat{k}_x \\ -\hat{k}_x \hat{\eta}_Z \hat{k}_y & \hat{k}_x \hat{\eta}_Z \hat{k}_x \end{pmatrix} \right\} \begin{pmatrix} \phi_x \\ \phi_y \end{pmatrix} = \omega^2 \begin{pmatrix} \phi_x \\ \phi_y \end{pmatrix}, \end{aligned} \tag{17}$$

which can be written in a more compact form as

$$[\mathcal{H}_\parallel (q^2 + K) + \mathcal{K}_Z]\phi = \omega^2 \phi, \tag{18}$$

where we have introduced two new matrices

$$\mathcal{H}_\parallel = \begin{pmatrix} \hat{\eta}_X & 0 \\ 0 & \hat{\eta}_Y \end{pmatrix}, \quad \mathcal{K}_Z = \begin{pmatrix} \hat{k}_y \hat{\eta}_Z \hat{k}_y & -\hat{k}_y \hat{\eta}_Z \hat{k}_x \\ -\hat{k}_x \hat{\eta}_Z \hat{k}_y & \hat{k}_x \hat{\eta}_Z \hat{k}_x \end{pmatrix}. \tag{19}$$

The eigenvalue equation for q,

$$[\mathcal{E}_\parallel (\omega^2 - \mathcal{K}_Z) - K]\phi = q^2 \phi, \tag{20}$$

is obtained by multiplying Eq. (18) by the matrix

$$\mathcal{E}_\parallel = \begin{pmatrix} \hat{\varepsilon}_X & 0 \\ 0 & \hat{\varepsilon}_Y \end{pmatrix}, \tag{21}$$

which is the inverse of $\mathcal{H}_\parallel$.

In the second situation we are considering, the dielectric tensor is not diagonal, but it has at least one fixed principal axis that coincides with the growth direction z. Thus, the tensor assumes the block diagonal form

$$\boldsymbol{\epsilon}(\mathbf{r}) = \begin{pmatrix} \epsilon_{xx}(\mathbf{r}) & \epsilon_{xy}(\mathbf{r}) & 0 \\ \epsilon_{yx}(\mathbf{r}) & \epsilon_{yy}(\mathbf{r}) & 0 \\ 0 & 0 & \epsilon_z(\mathbf{r}) \end{pmatrix}. \tag{22}$$

We indicate by $\mathcal{E}_{xy}$ the matrix that contains the Fourier coefficients of the dielectric tensor components in the x-y plane:

$$\mathcal{E}_{xy} = \begin{pmatrix} \hat{\varepsilon}_{XX} & \hat{\varepsilon}_{XY} \\ \hat{\varepsilon}_{YX} & \hat{\varepsilon}_{YY} \end{pmatrix}, \tag{23}$$

where $\hat{\varepsilon}_{XX}$, $\hat{\varepsilon}_{XY}$, $\hat{\varepsilon}_{YX}$, and $\hat{\varepsilon}_{YY}$ can be obtained in the usual way from Eq. (2) for the corresponding dielectric tensor elements. It is trivial to prove that the eigenvalue Eq. (20) can be directly written in the form

$$[\mathcal{E}_{xy} (\omega^2 - \mathcal{K}_Z) - K]\phi = q^2 \phi. \tag{24}$$

It is worth noticing that the only assumption here is that $\boldsymbol{\epsilon}(\mathbf{r})$ has the block form (22). Thus, in principle, the formulation given in Eq. (24) is also valid in the presence of ab-

sorption or optical activity, when the dielectric tensor is complex and, in general, not symmetric. This also includes the case in which the layer is composed of one or more birefringent media, for which the orientation of the principal axis in the x-y plane depends on the position in the unit cell. An example is a structure infiltrated with liquid crystals, where the molecule orientation depends on the void shape or can be controlled by an external electric field.[33] In all these situations, the calculation of the scattering matrix involves only two more Fourier transforms [for the off-diagonal elements $\epsilon_{xy}(\mathbf{r})$ and $\epsilon_{yx}(\mathbf{r})$] than in the previous case. In principle, this is not a problem. Nevertheless, if we want to evaluate the field distribution in the structure, and not only reflectance or transmittance, the inverse of $\mathcal{E}_{xy}$ is necessary. Since this operation can require much computational time, as we observed in Sec. II, when possible, a more efficient formulation of the matrix inversion problem is preferable.

An elegant solution is found when all the birefringent media in a given layer share the same principal axes and

$$E_{xy}(\mathbf{r}) = \begin{pmatrix} \epsilon_{xx}(\mathbf{r}) & \epsilon_{xy}(\mathbf{r}) \\ \epsilon_{xy}(\mathbf{r}) & \epsilon_{yy}(\mathbf{r}) \end{pmatrix} \tag{25}$$

is real and symmetric. A particularly simple example would be a structure composed of air and a biaxial medium where the principal axes in the x-y plane are rotated around the z axis by an angle ψ measured from the x axis of the laboratory reference Σ_{xyz} (see Fig. 1). Of course, one could work directly in the frame Σ_{XYZ}, but that would not be convenient because the Fourier transform of the dielectric tensor components would be unnecessarily complicated. Instead, we can write

$$E_{xy}(\mathbf{r}) = \mathbf{O}^{-1} \begin{pmatrix} \epsilon_X(\mathbf{r}) & 0 \\ 0 & \epsilon_Y(\mathbf{r}) \end{pmatrix} \mathbf{O}, \tag{26}$$

where ϵ_X and ϵ_Y are the eigenvalues of E_{xy}, and the diagonalizing matrix

$$\mathbf{O} = \begin{pmatrix} \cos\psi & -\sin\psi \\ \sin\psi & \cos\psi \end{pmatrix} \tag{27}$$

is orthogonal (that is, $\mathbf{O}^{-1}=\mathbf{O}^T$) and describes the anticlockwise rotation around $\hat{z}$ with respect to Σ_{xyz}.[34] Using the linearity properties of the Fourier transform, it is easy to demonstrate that

$$\mathcal{E}_{xy} = \mathbf{O}^{-1}\mathcal{E}_{\|}\mathbf{O} = \mathbf{O}^T\mathcal{E}_{\|}\mathbf{O}, \tag{28}$$

$$\mathcal{H}_{xy} = \mathbf{O}^{-1}\mathcal{H}_{\|}\mathbf{O} = \mathbf{O}^T\mathcal{H}_{\|}\mathbf{O}, \tag{29}$$

where $\mathcal{E}_{\|}$ indicates the diagonal form of $\mathcal{E}_{xy}$, and

$$\mathcal{H}_{xy} = \mathcal{E}_{xy}^{-1} \quad \text{and} \quad \mathcal{H}_{\|} = \begin{pmatrix} (\varepsilon_X)^{-1} & 0 \\ 0 & (\varepsilon_Y)^{-1} \end{pmatrix}, \tag{30}$$

with ε_X and ε_Y being the Fourier transform of ϵ_X and ϵ_Y, respectively.

It is worth noticing that the new eigenvalue problems (20) and (24) can be reduced to a generalized symmetric one for a centrosymmetric unit cell and, more generally, to a generalized Hermitian one for a real dielectric function. It follows that the particular orthogonality relations presented in Sec. II are still valid, and they are simply generalized to

$$\phi_i^T(\omega^2 - \mathcal{K}_Z)\phi_j = \delta_{ij} \tag{31}$$

and

$$\phi_i^\dagger(\omega^2 - \mathcal{K}_Z)\phi_j = \delta_{ij} \tag{32}$$

for symmetric and Hermitian problems, respectively. As we have shown in the previous section, these relations are extremely convenient in reducing the computational time for the construction of the interface matrix.

Once the unbounded problem is solved for each layer, the interface matrices are found following the procedure described in Sec. II provided the simple substitution of $\mathcal{K}$ with $\mathcal{K}_Z$. Finally, the iterative procedure for the construction of the scattering matrix is identical to the one presented earlier,[11] which is reported in the Appendix for completeness.

The problem of a layer grown along a direction that is not along a principal axis of the dielectric tensor will not be treated. Even though this represents certainly a possible and interesting situation, the solution of the problem is more complicated due to the mixing between the in-plane and the vertical components of the electric field in Eq. (A4). A description by means of a scattering-matrix theory would require an almost total reformulation of the eigenvalue problem that is beyond the scope of this paper.

IV. ASYMMETRIC UNIT CELL PHOTONIC CRYSTAL SLAB

In this section, we present a brief study of a periodically patterned system with a unit cell that lacks inversion symmetry. In particular, we show how the scattering-matrix method can be used to evaluate the band dispersion of a photonic crystal slab above and below the light line. The structure is composed of a high-refractive-index membrane of thickness d that is patterned with a triangular lattice of triangular holes, as schematically shown in Fig. 2. The triangles are taken to be equilateral with basis side of length L, and the triangular lattice has period a. The lattice and the unit cell are invariant under rotation by 120°, even though the system is not centrosymmetric as it would be for circular holes. The symmetry directions of the lattice are the usual ones for the triangular lattice.[35] Although the refractive index dispersion can be easily included in the calculation, here we assume a fixed dielectric constant $\epsilon=12.11$, which corresponds to the value for silicon at the usual telecommunication wavelength $\lambda=1.55$ μm.

In Figs. 3 and 4, we present the calculated reflectance for TE [Figs. 3(a) and 4(a)] and TM [Figs. 3(b) and 4(b)] as a function of (a/λ) and for different angles of incidence along Γ-K and Γ-M, respectively; the curves are slightly shifted for clarity. The resonances, which are clearly visible in the spectra, denote a coupling between the incoming beam and the photonic radiative modes of the slabs. It has been shown that angle-resolved reflectance or transmittance experiments allow for a direct measurement of the photonic band dispersion, through a study of the evolution of these resonant fea-

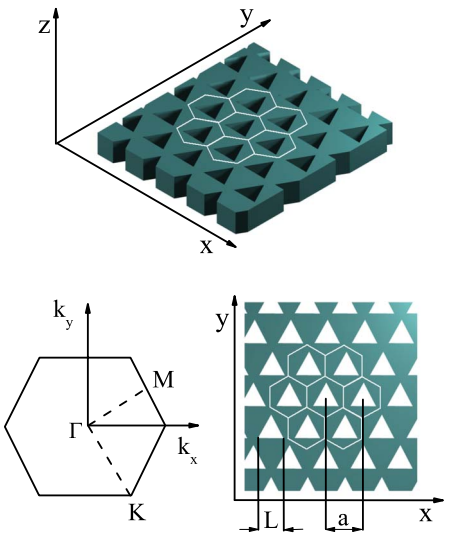

FIG. 2. (Color online) Scheme of a periodically patterned membrane of thickness d; the triangular lattice has period a, while the triangular hole's side measures L. The Brillouin zone for the triangular lattice is also shown together with the main symmetry directions.

tures as a function of the angle of incidence.[36–38]

Along Γ-K, the modes can be classified as even (TE-like) and odd (TM-like) with respect to the operator $\hat{\sigma}_{xy}$, which describes the reflection through a mirror plane bisecting the membrane. However, they are not purely TE or purely TM with respect to the plane of incidence for light incoming from the surface: this is evident by comparing the spectra in Fig. 3, where many of the features associated with odd and even modes are clearly present for incident fields of both polarizations. Yet in Fig. 4 we observe that if a mode appears in the TE reflectance spectra, it is not excited by TM-polarized incident light, and vice versa. This is a consequence of the higher symmetry along the $\Gamma-M$ direction, which makes possible also a classification according to the mode polarization or, equivalently, to the parity under mirror symmetry $\hat{\sigma}_{kz}$ with respect to the plane of incidence containing both $\mathbf{k}$ and $\hat{z}$; the parity can be either even ($\hat{\sigma}_{kz}=+1$, TM) or odd ($\hat{\sigma}_{kz}=-1$, TE).

In Figs. 3(c) and 4(c), we report the photonic band dispersion calculated by means of a guided-mode expansion (GME) method.[13] The calculations show the presence of photonic band gaps at ω and 2ω for quasi-TE and quasi-TM modes, respectively. This interesting feature makes the triangular lattice of triangular holes appealing for achieving enhancement of doubly resonant second-harmonic generation in photonic crystal slabs. In the design of such a structure, the GME method is a very powerful tool, since the calculations are much faster than those using the scattering matrix. Nevertheless, the method employs some approximations, the accuracy of which has to be verified by a comparison with a method that is exact within numerical error.[8,13,39] In this sense, the extension of the scattering-matrix method provides an important test of the application of the GME method to triangular lattices of triangular holes. We find that the guided-mode expansion results are in good agreement with scattering-matrix calculations in all the regimes that have been considered, including the high energy region of the quasi-TM band gaps, in which the GME approximations could possibly be less accurate.

Another interesting application of the scattering-matrix method is to evaluate the guided modes of the slab. Since these modes lie below the light line, they cannot be studied by simple angle-resolved reflectance or transmittance experiments.[40] An efficient method for exciting the guided modes is to work in attenuated total reflection (ATR) configuration. This technique is very well known for the study of surface plasmon polaritons, which can be excited by coupling the incoming beam through a prism.[41,42] The idea of using angle-resolved attenuated total reflectance for studying guided-mode dispersion in photonic crystal structures has been suggested and experimentally demonstrated by Galli *et al.*[43,44] A guided mode is found in correspondence with a dip in the reflectance spectrum, the strength and width of which are related to the mode losses and to the coupling efficiency with the incoming beam, which depends on the distance between the prism and the guide. For a sufficiently large distance of the prism from the slab, the position of the resonances tends to the ones of the guided mode. Following the same strategy,[43] we have simulated an experiment in ATR configuration for the patterned membrane using a silicon prism, which is located at a distance $0.7a$ from the slab. If we work above the critical angle $\theta_c=\arcsin(1/n_{\mathrm{Si}})=16.7°$, the reflectance is almost 1 everywhere and only a small fraction of the incident beam is diffracted into the prism for most frequencies. Nevertheless, an enhancement of the diffraction, and, consequently, a decrease in the reflection, is expected when a guided mode is excited. Using this method, we are able to map the guided-mode dispersion relation by looking at the dips in the ATR spectrum as a function of the angle of incidence θ and by defining the in-plane wave vector as $k=n_{\mathrm{prism}}(\omega/c)\sin\theta+G$, where n_{prism} is the refractive index of the prism material and G is a reciprocal lattice vector.

In Fig. 5(a), we report the photonic band dispersion of the slab along the direction Γ-K evaluated by means of the GME method. A scattering-matrix calculation as a function of the frequency at certain angle of incidence θ corresponds to scanning for guided modes along a virtual light line, the dispersion of which is given by $k=(2\pi/\lambda)\sin\theta$. Reflectance spectra for $\theta=20°$ along Γ-K for TE- and TM-polarized incident fields are shown in Fig. 5(b). This angle value is slightly above the critical angle $\theta_c=16.7°$ for silicon/air interface. The reflectance is almost 1 everywhere, except when the incident light is coupled to a guided mode. As in the case of the calculation above the light line, it is not possible to classify the modes according to the field polarization. As a consequence, many of the features are clearly visible for both polarizations. The width of each resonance is proportional to the mode losses due to the coupling; thus, the modes that appear narrower are the ones characterized by larger field confinement and, hence, weaker coupling to leaky modes through the prism.

V. POROUS SILICON SLOT WAVEGUIDE

Porous silicon is a very promising material for obtaining efficient silicon based light sources that are compatible with

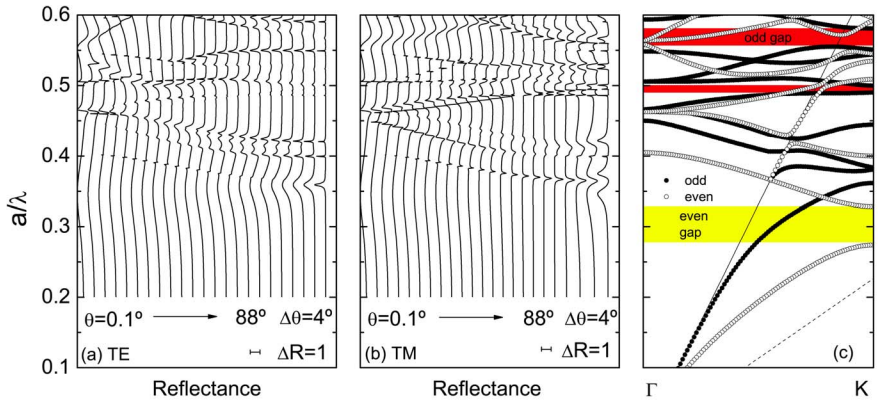

FIG. 3. (Color online) Reflectance calculations along Γ-K for (a) TE and (b) TM polarizations for a photonic crystal slab with a triangular pattern of triangular holes with $L/a=0.8$, $d/a=0.5$, and $\epsilon=12.11$. The curves are slightly shifted ($\Delta R=1$) for clarity. (c) Photonic band dispersion along Γ-K for even (open circle) and odd (full circle) modes with respect to the symmetry $\hat{\sigma}_{xy}$; photonic gaps are also indicated. The photon dispersion relation in air and in the effective core layer are given by solid and dashed lines, respectively.

complementary metal-oxide-semiconductor technology. Emission at telecommunication wavelengths has already been observed in erbium doped PSi planar microcavities.[45,46] In this section, we use the birefringent media theory presented in Sec. III to describe the optical properties of a PSi structure that could be suitable for efficient light emitters. The design does not require the evaluation of emission efficiency, and can be done by simply considering the passive properties of the device, such as its reflectance spectra and the electromagnetic field distribution within it.

The most common strategy for achieving large emission efficiency is to increase the electromagnetic field confinement in the region where the emitters are located. This is usually done by means of planar or two-dimensional photonic crystal microcavities.[47,48] An alternative route is to embed the emitter in a waveguide and to exploit the coupling with a guided mode. It has been recently demonstrated that large field confinements, below the diffraction limit, can be obtained for TM modes in the so-called slot waveguide, where a tiny (typically 10–20 nm thick) low index layer is realized in the core of the guide.[28] Due to the strong discontinuity of the normal field component at the interfaces with the slot, the fundamental TM mode is mainly localized in the low index region, leading to an enhancement of the emission into this mode.[29] In this case, the light is mainly emitted into the waveguide but in many applications vertical emission is preferable. A redistribution of the emitted light in the direction $\hat{z}$ normal to the surface is achievable in periodically patterned waveguides when the guided mode is folded in the first Brillouin zone above the light line at the Γ point.[49,50] Porous silicon is a good material for the realization of a slot waveguide, but the etching of the system can increase the losses due to the porous nature of the material. Thus, we prefer using a dielectric grating on the top of the waveguide in order to out-couple the guided modes [see Fig. 6(a)]. It is worth noting that nearly at normal incidence the field lies almost totally in the plane; on the contrary, for the TM guided mode, it is mainly oriented along z and, in particular, only this component is affected by refractive index discontinuity in the slot. For TM-polarized incident beam, the field components x and z experience two different dielectric constants $\epsilon_{\parallel}$ and $\epsilon_{\perp}$, respectively, and they are coupled by the

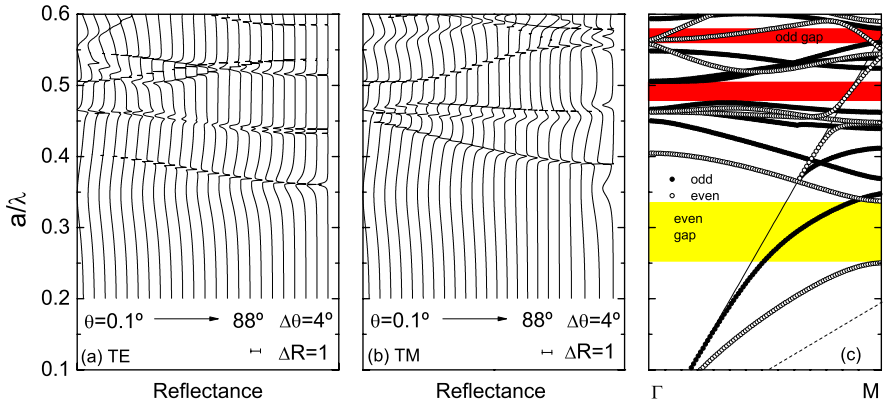

FIG. 4. (Color online) Reflectance calculations along Γ-M for (a) TE and (b) TM polarizations for a photonic crystal slab with a triangular pattern of triangular holes with $L/a=0.8$, $d/a=0.5$, and $\epsilon=12.11$. The curves are slightly shifted ($\Delta R=1$) for clarity. (c) Photonic band dispersion along Γ-M for even (open circle) and odd (full circle) modes with respect to the symmetry $\hat{\sigma}_{xy}$; photonic gaps are also indicated. The photon dispersion relations in air and in the effective core layer are given by solid and dashed lines, respectively.

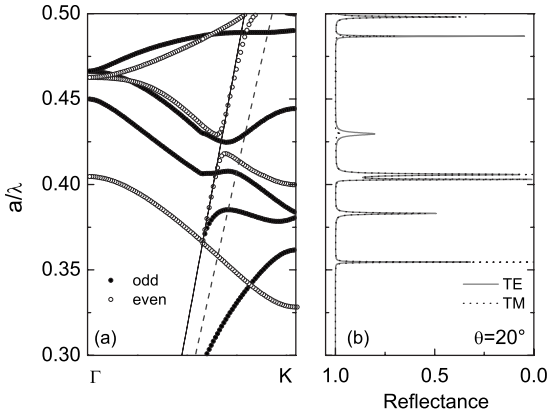

FIG. 5. (a) Photonic band dispersion for even (open circle) and odd (full circle) modes along Γ-K of a photonic crystal slab with a triangular pattern of triangular holes with $L/a=0.8$, $d/a=0.5$, and $\epsilon=12.11$. The photon dispersion relation in air is indicated by the solid line. The dashed line represents the effective light line for an angle of incidence $\theta=20°$ using a silicon prism; its distance from the slab is $0.7a$. (b) Attenuated total reflectance spectra along Γ-K for TE (line) and TM (dashed) polarizations at $\theta=20°$.

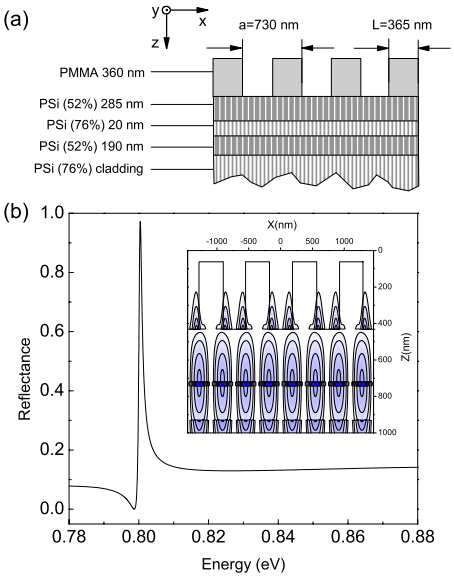

FIG. 6. (Color online) (a) Structure scheme and parameters. (b) Main panel: reflectance calculation for TM mode at angle of incidence $\theta=0.1°$ as a function of energy. Inset: contour plot of $|E_z|^2$ at wavelength $\lambda=1.55$ μm and $\theta=0.1°$ for TM polarized incident field.

grating. Thus, the description of the system requires a theory that takes into account the dielectric tensor anisotropy.

The medium is uniaxial, with a Maxwell-Garnett effective medium theory $\epsilon_X=\epsilon_Y=\epsilon_\parallel$ and $\epsilon_Z=\epsilon_\perp$ in Eq. (13) given by[27]

$$\frac{\epsilon_\parallel-\epsilon_{\mathrm{Si}}}{\epsilon_\parallel+\epsilon_{\mathrm{Si}}}=p\frac{1-\epsilon_{\mathrm{Si}}}{1+\epsilon_{\mathrm{Si}}}, \tag{33}$$

$$\epsilon_\perp-\epsilon_{\mathrm{Si}}=p(1-\epsilon_{\mathrm{Si}}), \tag{34}$$

where ϵ_{Si} and p are the silicon dielectric constant and the porosity, respectively. The porous silicon waveguide that is considered has the following composition: the lower cladding is high porosity silicon (p=0.76), the core consists of a low index slot (20 nm and p=0.76) embedded between two high index (p=0.56) layers of 190 and 285 nm width for the bottom and the top one, respectively. The coupler on the top of the waveguide is taken to be a polymethyl methacrylate (PMMA) ($n=1.5$) one-dimensional grating of 360 nm height with a period of 730 nm period and a filling factor $L/a=0.5$ [see Fig. 6(a)].

The reflectance spectra at near normal incidence ($\theta=0.1°$) for TM polarization as a function of the energy are shown in Fig. 6(b). The well-defined resonance at 0.8 eV (1.55 μm) corresponds to the excitation of the waveguide fundamental TM mode, which is made quasiguided by the grating. Since the patterned region does not extend in the core of the waveguide, the grating is essentially a perturbation of the mode. This is clear by looking at the inset of Fig. 6(b), where $|E_z|^2$ for an incident beam at $\lambda=1.55$ μm. The field distribution reminds one of the fundamental TM mode and, as it is expected, E_z is strongly confined in the slot due to the different layer porosities that determines the large discontinuity of the refractive index along z. This simple analysis suggests that if an emitter is placed in the slot region, enhancement of spontaneous emission in the vertical direction can be expected. A detailed analysis of the problem requires a calculation of the emission spectra. This can be done using the scattering-matrix theory proposed in Ref. 11, but the birefringence effects have to be included by following the strategy that has been proposed in Sec. III.

VI. CONCLUSION

A scattering-matrix method[11] for a periodically patterned multilayer has been extended to treat systems with asymmetric unit cells, and constituted of birefringent materials. In both cases, a detailed formulation of the method and original examples have been given in the paper. These results increase the flexibility of the formalism, which can be applied to multilayers with an arbitrary periodic pattern.

By exploiting properties of the eigenvectors, it is possible to keep the numerical efforts at a reasonable level, even when the unit cell lacks inversion symmetry. An application to a photonic crystal slab with a triangular lattice of triangular holes has been discussed. This structure is particularly interesting for the presence of photonic band gaps at ω and 2ω, which makes the system appealing for nonlinear optics. We considered angle-resolved reflectance and attenuated total reflectance for a description of the system above and below the light line.

Furthermore, the formalism is now suitable for the description of systems composed of one or more birefringent media when the growth direction is along one of the dielectric tensor principal axes. As an application, we studied a PSi slot waveguide with a one-dimensional periodic grating where large field confinement, below the diffraction limit, can be obtained for the TM mode. The description of the coupling through a dielectric grating requires a formalism

that takes into account the dielectric tensor anisotropy.

These results are relevant in view of investigation by means of a scattering-matrix method of several interesting systems that were not accessible through the original formulation of the method.

ACKNOWLEDGMENTS

The authors are grateful to Marisa Grieco and Sharon Weiss for their support and stimulating discussions.

APPENDIX: SCATTERING-MATRIX METHOD

In this appendix, we summarize the procedure for building the scattering matrix method of a periodically patterned multilayer. Here, we adopt the same notation as that of Whittaker and Culshaw,[11] assume a harmonic time dependence of the fields $e^{-i\omega t}$, and rescale $\omega\epsilon_0\mathbf{E}\rightarrow\mathbf{E}$ and $\omega/c\rightarrow\omega$. It follows that the two curl Maxwell's equations become

$$\nabla\times\mathbf{H}=-i\epsilon(\mathbf{r})\mathbf{E}, \tag{A1}$$

$$\nabla\times\mathbf{E}=i\omega^2\mathbf{H}, \tag{A2}$$

where $\mathbf{r}=(x,y)$ and $\epsilon(\mathbf{r})$ is periodic. Fourier series are introduced:

$$\mathbf{H}(\mathbf{r},z)=\sum_{\mathbf{G}}\tilde{\mathbf{H}}_{\mathbf{k}}(\mathbf{G},z)e^{i(\mathbf{k}+\mathbf{G})\cdot\mathbf{r}}, \tag{A3}$$

where $\mathbf{G}$ is the reciprocal lattice vector and $\mathbf{k}$ is a given wave vector; it is useful to introduce the vectors $\mathbf{h}(z)=[\tilde{\mathbf{H}}_{\mathbf{k}}(\mathbf{G}_1,z),\tilde{\mathbf{H}}_{\mathbf{k}}(\mathbf{G}_2,z),\ldots]^T$ for the magnetic field and $\mathbf{e}(z)=[\tilde{\mathbf{E}}_{\mathbf{k}}(\mathbf{G}_1,z),\tilde{\mathbf{E}}_{\mathbf{k}}(\mathbf{G}_2,z),\ldots]^T$ for the electric field Fourier components.

The matrix $\hat{\varepsilon}$ [see Eq. (2)] contains the Fourier components of the dielectric function and is taken to be $N\times N$, where N is the number of reciprocal lattice vectors considered in the calculation. A detailed discussion regarding the appropriate cutoff in the set of reciprocal lattice vectors has been given in Ref. 11.

Equations (A1) and (A2) yield

$$\begin{aligned}
i\hat{k}_y h_z(z)-h_y'(z)&=-i\hat{\varepsilon}e_x(z),\\
h_x'(z)-i\hat{k}_x h_z(z)&=-i\hat{\varepsilon}e_y(z),\\
i\hat{k}_x h_y(z)-i\hat{k}_y h_x(z)&=-i\hat{\varepsilon}e_z(z),\\
i\hat{k}_y e_z(z)-e_y'(z)&=i\omega^2 h_x(z),\\
e_x'(z)-i\hat{k}_x e_z(z)&=i\omega^2 h_y(z),\\
i\hat{k}_x e_y(z)-i\hat{k}_y e_x(z)&=i\omega^2 h_z(z),
\end{aligned} \tag{A4}$$

where $\hat{k}_x$ and $\hat{k}_y$ are diagonal matrices, $(\hat{k}_x)_{ii}=(k_x+G_{i,x})$ and $(\hat{k}_y)_{ii}=(k_y+G_{i,y})$, and the prime indicates the derivative with respect to z.

By solving the band structure for each unbounded layer, it is possible to construct a basis of propagating waves. The magnetic field can be expanded as

$$\mathbf{H}(\mathbf{r},z)=\sum_{\mathbf{G}}\left(\phi_x(\mathbf{G})\left[\hat{\mathbf{x}}-\frac{1}{q}(k_x+G_x)\hat{\mathbf{z}}\right]+\phi_y(\mathbf{G})\left[\hat{\mathbf{y}}-\frac{1}{q}(k_y+G_y)\hat{\mathbf{z}}\right]\right)e^{(\mathbf{k}+\mathbf{G})\cdot\mathbf{r}}e^{iqz}, \tag{A6}$$

where $\hat{\mathbf{x}}$, $\hat{\mathbf{y}}$, and $\hat{\mathbf{z}}$ give the direction of the coordinate axes, and $\phi_x(\mathbf{G})$ and $\phi_y(\mathbf{G})$ are the expansion coefficients. This is equivalent to

$$\mathbf{h}(z)=e^{iqz}\left\{\phi_x\hat{\mathbf{x}}+\phi_y\hat{\mathbf{y}}-\frac{1}{q}(\hat{k}_x\phi_x+\hat{k}_y\phi_y)\hat{\mathbf{z}}\right\}. \tag{A7}$$

From Eq. (A5) follows

$$\mathbf{e}(z)=\frac{1}{q}\hat{\eta}e^{iqz}\{[\hat{k}_y\hat{k}_x\phi_x+(q^2+\hat{k}_y\hat{k}_y)\phi_y]\hat{\mathbf{x}}-[\hat{k}_x\hat{k}_y\phi_y+(q^2+\hat{k}_x\hat{k}_x)\phi_x]\hat{\mathbf{y}}+q[\hat{k}_y\phi_x-\hat{k}_x\phi_y]\hat{\mathbf{z}}\}, \tag{A8}$$

where $\hat{\eta}$ contains the Fourier components of $\eta(\mathbf{r})=\epsilon^{-1}(\mathbf{r})$. Combining Eqs. (A5), (A7), and (A8) in Eqs. (A4), after a little algebra, we arrive at the eigenvalue equation

$$[\mathcal{E}(\omega^2-\mathcal{K})-K]\phi=q^2\phi, \tag{A9}$$

where $\phi=(\phi_x,\phi_y)^T$ and the $2N\times 2N$ matrices $\mathcal{E}$, K, and K are

$$\mathcal{E}=\begin{pmatrix}\hat{\varepsilon} & 0\\ 0 & \hat{\varepsilon}\end{pmatrix},\quad \mathcal{K}=\begin{pmatrix}\hat{k}_y\hat{\eta}\hat{k}_y & -\hat{k}_y\hat{\eta}\hat{k}_x\\ -\hat{k}_x\hat{\eta}\hat{k}_y & \hat{k}_x\hat{\eta}\hat{k}_x\end{pmatrix},$$

$$K=\begin{pmatrix}\hat{k}_x\hat{k}_x & \hat{k}_x\hat{k}_y\\ \hat{k}_y\hat{k}_x & \hat{k}_y\hat{k}_y\end{pmatrix}, \tag{A10}$$

where $\mathcal{K}K=0$ for an arbitrary η. The latter property can be exploited in order to write Eq. (A9) as a generalized eigenvector problem

$$[(\omega^2-\mathcal{K})\mathcal{E}(\omega^2-\mathcal{K})-\omega^2K]\phi=q^2(\omega^2-\mathcal{K})\phi. \tag{A11}$$

Using the basis set $\{\phi_i\}$, the magnetic field tangential components are expressed in the momentum representation as

$$\begin{pmatrix}h_x(z)\\ h_y(z)\end{pmatrix}=\sum_n\begin{pmatrix}\phi_{x_n}\\ \phi_{y_n}\end{pmatrix}(a_n e^{iq_n z}+b_n e^{iq_n(d-z)}), \tag{A12}$$

where d is the layer thickness, and a_n and b_n are respectively the coefficients of the forward and backward going waves. Similarly, using Eq. (A8), analogous expressions for the electric field are obtained:

$$\begin{pmatrix} -e_y(z) \\ e_x(z) \end{pmatrix} = \sum_n \mathcal{H}[q_n^2 + K] \begin{pmatrix} \phi_{x_n} \\ \phi_{y_n} \end{pmatrix} \frac{1}{q_n} (a_n e^{iq_{n^z}} - b_n e^{iq_n(d-z)}). \tag{A13}$$

Setting $\mathcal{H}=\mathcal{E}^{-1}$, $h_{\|}(z)=[h_x(z),h_y(z)]^T$, $e_{\|}(z)=[-e_y(z),e_x(z)]^T$, $a=(a_1,a_2,\ldots)^T$, and $b=(b_1,b_2,\ldots)^T$, introducing matrices $\hat{f}_{nn}(z)=e^{iq_{n^z}}$, with , and a matrix Φ, the columns of which are the vectors ϕ_n, the compact form (5) results, where eigenvalue (A9) is used in order to replace $\mathcal{H}[q_n^2+K]\phi_n$ with $(\omega^2-\mathcal{K})\phi_n$. The matrix M translates the expansion coefficients $\{a_n\}$ and $\{b_n\}$ in the Fourier components of the tangential field.

When the unit cell has inversion symmetry, it can be shown that the eigenvectors ϕ_n satisfy the orthogonal relation (3) and it is easy to verify that

$$M^{-1} = \frac{1}{2} \begin{pmatrix} \hat{q}\Phi^T & \Phi^T(\omega^2 - \mathcal{K}) \\ -\hat{q}\Phi^T & \Phi^T(\omega^2 - \mathcal{K}) \end{pmatrix}. \tag{A14}$$

The field amplitudes at the interface between the lth and $(l+1)$th layers are related by the so-called interface matrix $I(l,l+1)$, which is obtained by imposing the continuity of the field tangential components and it is defined as

$$\begin{pmatrix} \hat{f}_l a_l \\ b_l \end{pmatrix} = I(l,l+1) \begin{pmatrix} a_{l+1} \\ \hat{f}_{l+1} b_{l+1} \end{pmatrix} \tag{A15}$$

$$= M_l^{-1} M_{l+1} \begin{pmatrix} a_{l+1} \\ \hat{f}_{l+1} b_{l+1} \end{pmatrix}, \tag{A16}$$

where the matrix $\hat{f}_l$ is defined such that $\hat{f}_l=\hat{f}_l(d_l)$.

The scattering matrix between two layers relates their forward and backward propagating amplitudes (a_l,b_l) and $(a_{l'},b_{l'})$ as

$$\begin{pmatrix} a_l \\ b_{l'} \end{pmatrix} = S(l,l') \begin{pmatrix} a_{l'} \\ b_l \end{pmatrix} = \begin{pmatrix} S_{11} S_{12} \\ S_{21} S_{22} \end{pmatrix} \begin{pmatrix} a_{l'} \\ b_l \end{pmatrix}. \tag{A17}$$

The total scattering matrix is built up by means of an iterative procedure which allows one to evaluate the matrix $S(l',l+1)$ once $S(l',l)$ is known:

$$S_{11}(l',l+1) = (I_{11} - \hat{f}_l S_{12}(l',l) I_{21})^{-1} \hat{f}_l S_{11}(l',l),$$

$$S_{12}(l',l+1) = (I_{11} - \hat{f}_l S_{12}(l',l) I_{21})^{-1} (\hat{f}_l S_{12}(l',l) I_{22} - I_{12}) \hat{f}_{l+1},$$

$$S_{21}(l',l+1) = S_{22}(l',l) I_{21} S_{11}(l',l+1) + S_{21}(l',l),$$

$$S_{22}(l',l+1) = S_{22}(l',l) I_{21} S_{12}(l',l+1) + S_{22}(l',l) I_{22} \hat{f}_{l+1}.$$

The starting point is to consider that $S(l,l)=1$. When the total scattering matrix $S(0,N)$ has been built, reflectance and transmittance spectra are easily found.

[1] S. J. McNab, N. Moll, and Y. A. Vlasov, Opt. Express **11**, 2927 (2003).
[2] Y. Akahane, T. Asano, B. Song, and S. Noda, Nature (London) **425**, 944 (2003).
[3] R. Bräuber and O. Bryngdahl, Opt. Commun. **100**, 1 (1993).
[4] L. Li, J. Opt. Soc. Am. A **14**, 2758 (1997).
[5] Ph. Lalanne, IEEE J. Quantum Electron. **38**, 800 (2002).
[6] L. Pilozzi, A. D'Andrea, and R. Del Sole, Phys. Rev. B **54**, 10751 (1996).
[7] S. G. Tikhodeev, A. L. Yablonskii, E. A. Muljarov, N. A. Gippius, and T. Ishihara, Phys. Rev. B **66**, 045102 (2002).
[8] D. Gerace, M. Agio, L. C. Andreani, and Ph. Lalanne, Opt. Quantum Electron. **37**, 277 (2005).
[9] A. David, H. Benisty, and C. Weisbuch, Phys. Rev. B **73**, 075107 (2006).
[10] David Yuk Kei Ko and J. C. Inkson, Phys. Rev. B **38**, 9945 (1988).
[11] D. M. Whittaker and I. S. Culshaw, Phys. Rev. B **60**, 2610 (1999).
[12] S. Takayama, H. Kitagawa, Y. Tanaka, T. Asano, and S. Noda, Appl. Phys. Lett. **87**, 061107 (2005).
[13] L. C. Andreani and D. Gerace, Phys. Rev. B **73**, 235114 (2006).
[14] M. Centini, C. Sibilia, M. Scalora, G. D'Aguanno, M. Bertolotti, M. J. Bloemer, C. M. Bowden, and I. Nefedov, Phys. Rev. E **60**, 4891 (1999).
[15] C. De Angelis, F. Gringoli, M. Midrio, D. Modotto, J. S. Aitchison, and G. F. Nalesso, J. Opt. Soc. Am. B **18**, 348 (2001).
[16] Y. Dumeige, I. Sagnes, P. Monnier, P. Vidakovic, I. Abram, C. Mériadec, and A. Levenson, Phys. Rev. Lett. **89**, 043901 (2002).
[17] M. Liscidini and L. C. Andreani, Appl. Phys. Lett. **85**, 1883 (2004).
[18] A. R. Cowan and Jeff F. Young, Phys. Rev. B **65**, 085106 (2002).
[19] L. T. Canham, Appl. Phys. Lett. **57**, 1046 (1990).
[20] L. Pavesi, Riv. Nuovo Cimento **20**, 1 (1997).
[21] C. Mazzoleni and L. Pavesi, Appl. Phys. Lett. **67**, 2983 (1995).
[22] D. G. Gusev, I. V. Soboleva, M. G. Martemyanov, T. V. Dolgova, A. A. Fedyanin, and O. A. Aktsipetrov, Phys. Rev. B **68**, 233303 (2003).
[23] J. Bertolotti, M. Galli, R. Sapienza, M. Ghulinyan, S. Gottardo, L. C. Andreani, L. Pavesi, and D. S. Wiersma, Phys. Rev. E **74**, 035602(R) (2006).
[24] Z. Gaburro, C. J. Oton, L. Pavesi, and L. Pancheri, Appl. Phys. Lett. **84**, 4388 (2004).
[25] J. J. Saarinen, S. M. Weiss, P. M. Fauchet, and J. E. Sipe, Opt. Express **13**, 3754 (2005).
[26] E. Guillermain, V. Lysenko, R. Orobtchouk, T. Benyattou, S. Roux, A. Pillonnet, and P. Perriat, Appl. Phys. Lett. **90**, 241116 (2007).
[27] J. E. Lugo, J. A. del Rio, and J. Taguena-Martinez, J. Appl. Phys. **81**, 1923 (1997).
[28] Qianfan Xu, Vilson R. Almeida, Roberto R. Panepucci, and Michal Lipson, Opt. Lett. **29**, 1626 (2004).
[29] M. Galli, D. Gerace, A. Politi, M. Liscidini, M. Patrini, L. C. Andreani, A. Canino, M. Miritello, R. Lo Savio, A. Irrera, and F. Priolo, Appl. Phys. Lett. **89**, 241114 (2006).

[30] J. P. Van der Ziel, Appl. Phys. Lett. **26**, 60 (1975).
[31] A. Fiore, V. Berger, E. Rosencher, P. Bravetti, and J. Nagle, Nature (London) **391**, 463 (1998).
[32] J. J. Saarinen, S. M. Weiss, P. M. Fauchet, and J. E. Sipe (unpublished).
[33] S. W. Leonard, J. P. Mondia, H. M. van Driel, O. Toader, S. John, K. Busch, A. Birner, U. Gosele, and V. Lehmann, Phys. Rev. B **61**, R2389 (2000).
[34] The same argument can be used when E_{xy} is hermitian. In this case, the diagonalizing matrix O is unitary, and its inverse $O^{-1} = O^{\dagger}$.
[35] The complex Fourier transform of the dielectric function for the triangular lattice of triangular holes can be found in Ref. 13.
[36] T. Fujita, Y. Sato, T. Kuitani, and T. Ishihara, Phys. Rev. B **57**, 12428 (1998).
[37] V. N. Astratov, D. M. Whittaker, I. S. Culshaw, R. M. Stevenson, M. S. Skolnick, T. F. Krauss, and R. M. De La Rue, Phys. Rev. B **60**, R16255 (1999).
[38] M. Patrini, M. Galli, F. Marabelli, M. Agio, L. C. Andreani, D. Peyrade, and Y. Chen, IEEE J. Quantum Electron. **38**, 885 (2002).
[39] L. C. Andreani and M. Agio, IEEE J. Quantum Electron. **38**, 891 (2002).
[40] N. Carlsson, T. Takemori, K. Asakawa, and Y. Katayama, J. Opt. Soc. Am. B **18**, 1260 (2001).
[41] H. Raether, *Surface Plasmons* (Springer, Berlin, 1988).
[42] *Surface Polaritons*, edited by V. M. Agranovich and D. L. Mills (North-Holland, Amsterdam, 1982).
[43] M. Galli, M. Belotti, D. Bajoni, M. Patrini, G. Guizzetti, D. Gerace, M. Agio, L. C. Andreani, and Y. Chen, Phys. Rev. B **70**, 081307(R) (2004).
[44] M. Galli, D. Bajoni, M. Patrini, G. Guizzetti, D. Gerace, L. C. Andreani, M. Belotti, and Y. Chen, Phys. Rev. B **72**, 125322 (2005).
[45] P. J. Reece, M. Gal, H. H. Tan, and C. Jagadish, Appl. Phys. Lett. **85**, 3363 (2004).
[46] S. M. Weiss, J. Zhang, P. M. Fauchet, V. V. Seregin, and J. L. Coffer, Appl. Phys. Lett. **90**, 031112 (2007).
[47] A. M. Vredenberg, N. E. J. Hunt, E. F. Schubert, D. C. Jacobson, J. M. Poate, and G. J. Zydzik, Phys. Rev. Lett. **71**, 517 (1993).
[48] Reginald K. Lee, Oskar Painter, Benjamin Kitzke, Axel Scherer, and Amnon Yariv, J. Opt. Soc. Am. B **17**, 629 (2000).
[49] M. Galli, A. Politi, M. Belotti, D. Gerace, M. Liscidini, M. Patrini, L. C. Andreani, M. Miritello, A. Irrera, F. Priolo, and Y. Chen, Appl. Phys. Lett. **88**, 251114 (2006).
[50] A. David, C. Meier, R. Sharma, F. S. Diana, S. P. DenBaars, E. Hu, S. Nakamura, C. Weisbuch, and H. Benisty, Appl. Phys. Lett. **87**, 101107 (2005).